Direct Synthesis of Well-Ordered and Unusually Reactive MnSBA-15 Mesoporous Molecular Sieves with High Manganese Content

M. Selvaraj*,†,‡ and T. G. Lee‡

Department of Chemical and Biomolecular Engineering, National University of Singapore, Singapore − 119260, and Department of Chemical Engineering, Yonsei University, Seoul 12-749, Korea

Received: June 24, 2006; In Final Form: August 9, 2006

The mesoporous MnSBA-15 materials with different n_{Si}/n_{Mn} ratios of 4, 8, 20, and 50 have been synthesized, for the first time, using manganese nitrate tetrahydrate and Pluronic 123 triblock polymer [$(EO)_{20}(PO)_{70}$-$(EO)_{20}$] by simply adjusting the molar ratio of water to hydrochloric acid (n_{H2O}/n_{HCl}) under direct hydrothermal conditions. For the effect of structural and textural properties with incorporation of manganese, the MnSBA-15 has been synthesized with different synthesis temperatures at the fixed molar ratios of $n_{Si}/n_{Mn} = 4$ and $n_{H2O}/n_{HCl} = 295$ in the synthesis gel. The hydrothermal and thermal stabilities of MnSBA-15 have also been investigated. The calcined MnSBA-15 materials prepared have been characterized by ICP-AES, XRD, N_2 adsorption, ESR, FE-SEM, and TEM. The ICP-AES studies show a higher amount of manganese incorporation on the silica pore walls, as MnSBA-15 with a n_{Si}/n_{Mn} ratio up to 2.2 can be successfully prepared at a fixed n_{H2O}/n_{HCl} molar ratio of 295 by adjusting the ratios of n_{Si}/n_{Mn} in the synthesis gel. The structural and textural properties of calcined MnSBA-15 prepared can be found by the results of XRD and N_2 adsorption. The investigation of ESR results clearly describe the effect of structure and Mn species coordination on the SBA-15 silica pore walls while the uniform pore diameter and rope-like hexagonal mesoporous structure of MnSBA-15 can be identified by TEM and FE-SEM images. With increasing synthesis temperature, an increase the unit cell parameter, pore size, and pore volume and a decrease the specific surface area and pore wall thickness of MnSBA-15 can be obviously noted by the results of XRD and N_2 adsorption. The hexagonal MnSBA-15 materials prepared could be tested as catalysts in epoxidation of *trans*-stilbene to produce *trans*-stilbene oxide under various optimal conditions while their catalytic properties could also be compared to the results of MnMCM-41 and ZrMnMCM-41.

Introduction

Manganese and its microporous molecular sieves have been attracting considerable attention due to their remarkable activity as catalysts for the selective epoxidation of olefins,[1,2] oxidation of SO_2,[3] and reduction of NO_x .[4] However, they are not useful for treating feeds and the production of more bulky fine chemicals, owing to their small pore size. These limitations were overcome with the discovery of mesoporous materials[5] which have greatly enlarged mesopores suitable as catalysts for organic reactions involving bulky molecules. Unfortunately, the acid strength of MCM-41 resembles that of the amorphous silica aluminas rather than that of the more strongly acidic zeolites[6] while their hydrothermal and thermal stabilities are very low due to thinner pore walls. Although the mesoporous material is valuable for many organic conversions,[7] enhancement of its acidity is desirable for extension of its applicability. For example, Selvaraj et al. reported the details of the synthesis and characterization of some mesoporous materials with increasing acid strength along with a good hydrothermal stability, and the materials were used as catalysts for the synthesis of fine chemicals.[8−11]

In the new family of mesoporous materials, SBA-15 materials synthesized with triblock copolymer as surfactant under strong acidic conditions exhibit larger pore sizes and thicker pore walls compared with M41S, while, their hydrothermal and thermal stabilities are higher as compared to MCM-41.[5,12−16] These materials have attracted much attention because of their interesting structures and potential applications in catalysis. However, they are all purely siliceous materials, and it is difficult to prepare heteroatom-introduced mesoporous silica under strongly acidic synthesis conditions. This is because, under such conditions, metals will exist only in the cationic form rather than their corresponding oxo species, and therefore heteroatoms cannot be introduced into the mesoporous walls via a condensation process with silicon species. As we know, the active sites in molecular sieves are always from heteroatoms; for example, the introduction of Al^{3+} and Ti^{4+} will provide acidic and redox sites into pure silica, respectively.[7,17] Therefore, it is of great importance to introduce heteroatoms into the walls of these mesoporous silica materials prepared under strongly acidic conditions. Several studies are dealing with the incorporation of heteroatoms such as Al,[18,] Fe,[19] V,[20] Ti,[21] and Ga[22] on SBA-15 by direct synthesis or an impregnation method to create active sites in these materials. Especially, Wu et al.,[23] for the first time, reported that the Al^{3+} and Ti^{4+} species were highly substituted into mesoporous SBA-15 molecular sieves by the "pH-adjusting" method in synthesis gel. However, to the best of our knowledge, synthesis of MnSBA-15 with a high amount of Mn framework on silica pore walls under direct hydrothermal method and its characterization have not been clearly reported in the open literature so far.

* To whom correspondence should be addressed. E-mail: chems@nus.edu.sg.
† National University of Singapore.
‡ Yonsei University.

10.1021/jp063957i CCC: $33.50
Published on Web 10/06/2006

In the present study, we describe, for the first time, the clearly understanding synthesis procedure to prepare the mesoporous MnSBA-15 molecular sieves with high manganese loadings. Typically, the MnSBA-15 materials have been synthesized with different n_{Si}/n_{Mn} ratios by simply adjusting the molar ratio of n_{H2O}/n_{HCl} in order to lower the pH of the synthesis medium under direct hydrothermal conditions. The MnSBA-15 has also been synthesized with various synthesis temperatures at fixed molar ratios of $n_{Si}/n_{Mn} = 4$ and $n_{H2O}/n_{HCl} = 295$ in the synthesis gel to find the effect of structural and textural properties and the incorporation of manganese. The hydrothermal and thermal stabilities of MnSBA-15 have also been investigated to be proven a higher catalytic activity. The above synthesized materials have been characterized by ICP-AES, XRD, N_2 adsorption, ESR, FE-SEM, and TEM for proof of the standard mesoporous SBA-15 materials, and their catalytic activity are tested as catalysts in the epoxidation of *trans*-stilbene (TS). MnSBA-15 catalysts are very active and give significantly higher conversion of TS and selectivity to *trans*-stilbene oxide (TSO) as compared to mono and bimetal substituted unidimensional MCM-41 materials.[2,24,25] Epoxidation of TS is an industrially important reaction because TSO is used as the main intermediate for the organic chemical synthesis in the fine chemical industries. Recently, Yonemitsu and Selvaraj et al.[2,24,25] have reported the epoxidation of TS over mono metal substituted MnMCM-41 and bimetallic substituted ZrMnMCM-41, and they have proposed that the moderate Lewis acidity of these catalysts is favorable for formation of TSO.

Experimental Section

1. Chemicals. All chemicals viz. triblock copolymer poly(ethylene glycol)-*block*-poly(propylene glycol)-*block*-poly(ethylene glycol) (Pluronic P123, molecular weight = 5800, $EO_{20}PO_{70}EO_{20}$), tetraethyl orthosilicate (TEOS), hydrochloric acid (HCl), manganese nitrate tetrahydrate ($Mn(NO_3)_4 \cdot 4H_2O$) were purchased from Aldrich Chemical Inc. All chemicals were used as received without further purification. Millipore water was used in all experiments.

2. Synthesis. The mesoporous MnSBA-15 molecular sieve materials were synthesized using a triblock copolymer poly(ethylene glycol)-*block*-poly(propylene glycol)-*block*-poly(ethylene glycol) (Pluronic P123, molecular weight = 5800, $EO_{20}PO_{70}EO_{20}$, Aldrich) as a structure directing agent. In a typical synthesis of MnSBA-15, 4 g of Pluronic P123 was dissolved in 25 mL of water to get a clear solution. Thereafter, the required amount of dilute HCl solution was added, and the solution was again stirred for another 1 h to be associated with the hydronium ions with the alkylene oxide units. Then, 9 g of tetraethyl orthosilicate and the required amount of $Mn(NO_3)_2 \cdot 4H_2O$ solution were added, and the resulting mixture was stirred for 24 h at 313 K. A first set of samples were prepared using a fixed n_{Si}/n_{Mn} ratio of 4 by changing the molar ratio of n_{H2O}/n_{HCl}, and it was denoted as MnSBA-15(*x*H), where *x* denotes the molar water to hydrochloric acid ratio (n_{H2O}/n_{HCl}). A second set of samples were prepared by changing the n_{Si}/n_{Mn} ratios (n_{Si}/n_{Mn} = 4, 8, 20, and 50) using a fixed n_{H2O}/n_{HCl} molar ratio of 295 (75 mL of 0.25 M HCl; it means 90 mL of H_2O with 0.93 mL of HCl). A third set of MnSBA-15 samples with a fixed n_{Si}/n_{Mn} molar ratio of 4, and n_{H2O}/n_{HCl} molar ratio of 295, were prepared by varying the synthesis temperature from 373 to 403 K. The samples were labeled MnSBA-15(*y*T), where *y* denotes the synthesis temperature. The solid products were recovered by filtration, washed several times by water with ethanol, and dried overnight at 373 K. The molar gel composition was 1 TEOS/0.02−0.25 MnO/0.016 P123/0.43−5.2 HCl/127−210 H_2O. Finally, the samples were calcined at 813 K in air at 6 h for complete removal of the template.

3. Evaluation of Hydrothermal and Thermal Stabilities. For investigation of hydrothermal stability the calcined MnSBA-15 in pure boiling water at 373 K for 168 h in autogenous pressure was treated. The same samples were again treated at 973 K for 12 h and 1123 K for 12 h for investigation of thermal stability.

4. Characterization. The elemental composition in the solid products were analyzed by ICP-AES (Perkin-Elmer, Optima 3000) after the samples were dissolved in a HF solution. The small-angle XRD patterns were recorded under ambient conditions on a Shimadzu XRD-6000 with Cu Kα radiation (λ = 1.5406 Å). The X-ray tube was operated at 40 kV and 30 mA while the diffractograms were recorded in the 2θ range of 0.6 to 10° with a 2θ step size of 0.01 and a step time of 10 s. Nitrogen adsorption/desorption measurements were conducted using Quantachrome Autosorb-1 by N_2 physisorption at 77 K. All samples were outgassed for 3 h at 250 °C under vacuum ($p < 10^{-5}$ hPa) in the degas port of the sorption analyzer. The BET specific surface areas of the samples were calculated in the range of relative pressures between 0.05 and 0.35. The pore size distributions were calculated from the adsorption branch of the isotherm using the thermodynamic-based Barrett−Joyner−Halenda (BJH) method. The total pore volume was determined from the adsorption branch of the N_2 isotherm at $P/P_0 = 1$. The pore wall thickness (t_w) was also calculated by unit cell parameter (a_0) and pore diameter (d_p). ESR spectra for the calcined samples were recorded at X-band at 298 K on a Bruker ESP 300 spectrometer. The magnetic field was calibrated with a Varian E-500 gaussmeter. The microwave frequency was measured by a Hewlett-Packard HP 5342A frequency counter. Field-emission scanning electron microscopy (FESEM) images were obtained with a JEOL JSM-6700F microscope at an accelerating voltage of 5.0 kV. Transmission electron microscopy (TEM) images were collected on a JEOL 2010 electron microscope operated at an acceleration voltage of 200 kV.

5. Catalytic Studies. *trans*-Stilbene (>98%) and *tert*-butyl hydroperoxide (TBHP) (70% aqueous solution) (Aldrich) were used as the reactants. Catalytic reactions were carried out according to the following procedure. Substrate, solvent, and catalyst were first introduced into a round-bottom flask. After oxidant was carefully added, the reaction was started by immersing the flask into a water bath kept at the reaction temperature. The reaction was carried out under violent stirring. All the products were quantified by a gas chromatograph (Shimadzu GC-14B) equipped with a BPX5 capillary column and an FID detector using toluene as an internal standard. *Tert*-butyl alcohol produced from TBHP was also analyzed, from which TBHP conversion was estimated. GC-MS (Shimadzu GCMS-QP5050A) and NMR (JEOL FT-NMR Lambda 400NMR) were also used to identify the products. For reusable experiments, the MnSBA-15 catalysts were reactivated in oxygen atmosphere at 773 K for 6 h.

Results and Discussions

Effect of n_{H2O}/n_{HCl} Molar Ratios. The mesoporous pure silica SBA-15 molecular sieve materials were synthesized under strongly acidic hydrothermal conditions ($n_{H2O}/n_{HCl} < 40$, i.e., pH < 1), and it is difficult to synthesize Mn-introduced SBA-15 with high amount Mn loadings because the Mn−O−Si bonds are easily dissociated due to increasing the hydrolysis rate of

manganese precursors with silicon precursors. But, lowering the acidity of the solution may decrease the hydrolysis rate of the manganese precursors to match that of the silicon precursors. This might enhance the interaction between the Mn−OH and Si−OH species in the synthesis gel, resulting in a higher amount of Mn-ion incorporation at high n_{H2O}/n_{HCl} ratio. Therefore, we have tried to synthesize a higher amount of Mn incorporation on SBA-15 silica pore walls by simply adjusting the n_{H2O}/n_{HCl} molar ratio from 40 to 295 in the gel in order to lower the pH medium without changing the structural integrity of parent SBA-15 materials. The following synthesis mechanism clearly explaines how to incorporate Mn on SBA-15 silica pore walls.

The incorporation of Mn species into SBA-15 by adjusting the molar n_{H2O}/n_{HCl} ratio can be explained by the synthesis mechanism of SBA-15 proposed by Zhao et al.[12,13] According to SBA-15 mechanism (eq 1), the formation of hexagonal mesophase under highly acidic hydrothermal conditions occurs through the $S^0\,H^+X^-I^+$ pathway (nonionic polymeric surfactant (S^+), halogen anions/counteranions (X^-), and the protonated inorganic SiO_2 species (I^+)). At very high pH synthesis medium (pH < 2), the alkylene oxide groups of the surfactant are clearly solubilized, and the hydronium ions are then associated with the alkylene oxide units while the silica species are positively charged by proton abstraction at low pH by adding the water and hydrochloric acid. The charge-associated alkylene oxide units and the cationic silica species are equally assembled together by a combination of electrostatic, hydrogen bonding, and van der Waals interactions $REO_{m-y}[(EO)\cdot H_3O^+]_y\cdots yX^-\cdots I^+$, which can be designated as $(S^0\ H^+)(X^-I^+)$. As already mentioned, at high pH synthesis medium the introduction of Mn is very difficult due to the high solubility of the Mn precursors. This can be explained by the following equations:

$$Mn(NO_3)_2(s) + 2H^+(aq) \rightleftarrows Mn^{2+}(aq) + 2HNO_3(aq) \quad (pH < 1.6) \quad (1)$$

$$2Mn^{2+} + 2H_2O \rightarrow 2Mn(OH)^+ + 2H^+ \quad (pH > 2) \quad (2)$$

On the basis of the above mechanism for synthesis of purely silica SBA-15, we have clearly observed that a high acidic medium is necessary for the formation of the hexagonal mesophase and a large uniform pore diameter on SBA-15, but it prohibits the introduction of Mn into SBA-15. Hence, we can be decided to optimize the pH of the synthesis medium by adjusting the n_{H2O}/n_{HCl} molar ratio. Initially, the formation of the hexagonal phase has been investigated after adjusting the pH in the synthesis gel between 0 and 1.7. Once the surfactant and silica species are protonated, the cationic silica species undergo partial condensation and form a mesostructure through the counteranion (X^-) with the cationic surfactant species; as a result, pH of the synthesis medium increases. It should be noted that when the n_{H2O}/n_{HCl} ratio is increased from 40 to 166, the pH of the synthesis gel would only go to a high of 1.8 even after a few hours of stirring and addition of the silicon and manganese sources, while the pH of the synthesis gel is around 2.3 when the n_{H2O}/n_{HCl} molar ratio is increased to 295 and it is above the zero net charge of silica. If the pH of the synthesis medium rises above the zero net charge of silica, the silica species are negatively charged which enhances the interaction with the $Mn(OH)^+$ species. Hence, the concentration of Mn hydroxyl species gradually increases in the synthesis gel with decreasing H^+ concentration in the synthesis gel (eq 2). Hence, the partially condensed silica species are able to form a Mn−O−Si bond with $Mn(OH)^+$ species at less concentration of H^+ in the synthesis gel while the structural order of the materials is maintained when formed at a pH of ca. 2.3. Moreover, it can be clearly observed that the heteroatom incorporation on SBA-15 silica walls depends on the concentration of H^+ ions. For the proof of mesoporous materials, the prepared calcined MnSBA-15 have been characterized by ICP-AES, XRD, N_2 adsorption, ESR, FE-SEM, and TEM.

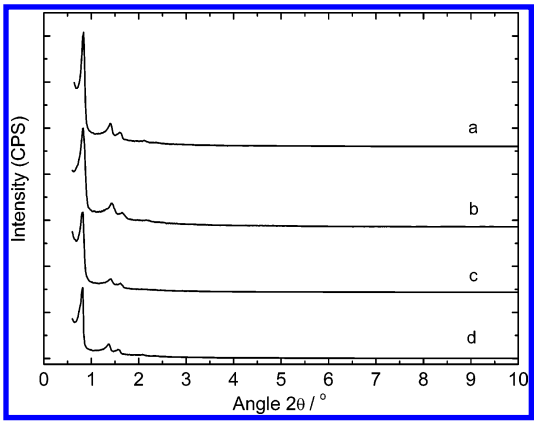

Figure 1. XRD powder patterns of calcined MnSBA-15 materials prepared with different n_{H2O}/n_{HCl} ratios: (a) MnSBA-15(40H), (b) MnSBA-15(70H), (c) MnSBA-15(166H), and (d) MnSBA-15(295H).

The powder XRD patterns of MnSBA-15 samples prepared using different water to hydrochloric acid molar ratios (n_{H2O}/n_{HCl}) are shown in Figure 1. The well-defined XRD patterns are similar to those recorded for all-silica SBA-15 materials as described by Zhao et al.[12,13] The XRD pattern of all MnSBA-15 materials exhibit five well-resolved peaks which are indexed to the (100), (110), (200), (210), and (300) reflections of the hexagonal *P*6*mm* space group. The length of the hexagonal unit cell a_0 is calculated using the formula $a_0 = 2d_{100}/\sqrt{3}$ from the *d* spacing values. The observed *d* spacing and unit cell parameter results are well-matched with the hexagonal *P*6*mm* space group. The length of the unit cell a_0 systematically increases from 121.0 to 124.2 Å when the n_{H2O}/n_{HCl} molar ratios are gradually increased from 40 to 295, and the intensity of XRD peaks decreases with increasing Mn incorporation. That is why, due to a larger ionic radius of Mn than Si, the Mn−O bond length is higher as compared to Si−O bond length. Moreover, it is found that the n_{Si}/n_{Mn} ratio of the product decreases from 48.3 to 2.2 with increasing molar ratio of n_{H2O}/n_{HCl}, and the results were found by the results of ICP-AES (Table 1). The above-described experimental results suggest that the "pH adjusting method" is necessary for a higher amount of Mn incorporation on the silica pore walls without affecting the structural order of the parent SBA-15 materials.

The N_2 adsorption−desorption isotherms and pore size distribution of calcined MnSBA-15 prepared with different water to hydrochloric acid molar ratios (n_{H2O}/n_{HCl}) are shown in Figure 2. The textural properties of the MnSBA-15 samples are given in Table 1. All isotherms are IV type according to the IUPAC classification and exhibited a H1-type broad hysteresis loop, which is typical of large-pore mesoporous solids.[26] As the relative pressure increases ($p/p_0 > 0.6$), all isotherms exhibit a sharp step characteristic of capillary condensation of nitrogen within uniform mesopores, where the p/p_0 position of the inflection point is correlated to the diameter of the mesopore. As SBA-15 has a hexagonal arrangement of mesopores connected by smaller micropores,[27] it is clear that the broad hysteresis loop in the isotherms of SBA-15 reflects the long mesopores, which limit the emptying and filling of the accessible volume.

TABLE 1: Physicochemical Properties and Synthesis Conditions of MnSBA-15[a]

catalysts	n_{H2O}/n_{HCl} (in molar ratio)	n_{Si}/n_{Mn} gel	n_{Si}/n_{Mn} product	T (K)	a_o (Å)	SA_{BET} (m^2/g)	V_p (cm^3/g)	D_p (Å)	T_w (Å)
MnSBA-15(40H)	40	4	48.3	373	121.0	870	1.05	85.7	35.3
MnSBA-15(70H)	70	4	26.3	373	122.8	910	1.07	86.7	36.1
MnSBA-15(166H)	166	4	7.2	373	123.5	930	1.09	86.8	36.7
MnSBA-15(295H)	295	4	2.2	373	124.2	998	1.12	86.9	37.3
MnSBA-15(4)	295	8	4.3	373	123.7	1010	1.11	86.7	37.0
MnSBA-15(10)	295	20	10.4	373	121.5	1035	1.10	86.5	35.0
MnSBA-15(26)	295	50	26.3	373	120.7	1079	1.08	86.2	34.5
MnSBA-15(383 K)	295	4	2.2	383	124.8	938	1.13	87.5	37.3
MnSBA-15(393 K)	295	4	2.3	393	125.1	900	1.14	87.9	37.2
MnSBA-15(403 K)	295	4	2.3	403	124.7	720	1.16	90.6	34.1

[a] The results of n_{Si}/n_{Mn} ratios in the products are determined by ICP-AES; a_0, unit cell parameter; A_{BET}, specific surface area; d_p, pore diameter; V_p, pore volume; pore wall thickness (t_w) = unit cell parameter (a_0) − pore diameter (d_p).

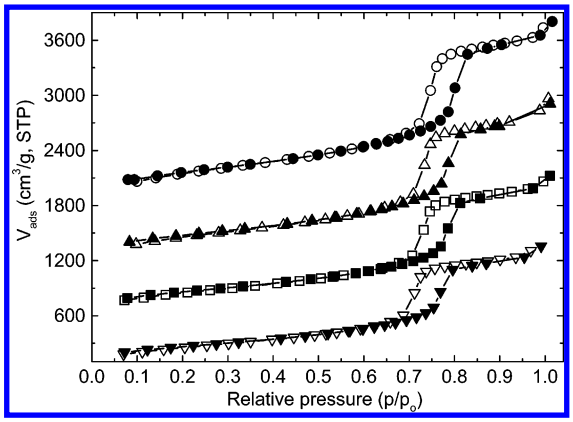

Figure 2. Nitrogen adsorption isotherms of calcined MnSBA-15 materials prepared with different n_{H2O}/n_{HCl} ratios (closed symbols, adsorption; open symbols, desorption): (▼) MnSBA-15(40H), (■) MnSBA-15(70H), (▲) MnSBA-15(166H), and (●) MnSBA-15(295H). (For the value of shift of each isotherm, the values of relative pressure (p/p_o) are 6.31, 6.42, 6.73, and 6.82 for MnSBA-15(40H), MnSBA-15(70H), MnSBA-15(166H), and MnSBA-15(295H), respectively.)

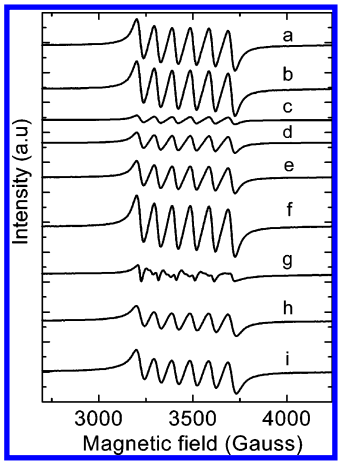

Figure 3. ESR spectra of calcined MnSBA-15 samples: (a) MnSBA-15(295H) at 1123 K, (b) MnSBA-15(295H) at 973 K, (c) MnSBA-15(26), (d) MnSBA-15(10), (e) MnSBA-15(4), (f) MnSBA-15(295H), (g) MnSBA-15(40H), (h) MnSBA-15(70H), and (i) MnSBA-15(166H).

Textural properties such as specific surface area, pore diameter, and specific pore volume of the MnSBA-15 samples systematically increase with gradually increasing the molar ratio of n_{H2O}/n_{HCl}. A lower specific surface area is 870 m^2/g for MnSBA-15(40H); but, for MnSBA-15(295H), a higher surface area is 998 m^2/g while the specific pore volume and pore wall thickness for the corresponding samples increases from 1.05 to 1.12 cm^3/g, and 35.3 to 37.3 Å, respectively. The pore diameter of MnSBA-15(295H) is 86.9 Å, which is 1.2 Å higher as compared to the sample prepared at very low n_{H2O}/n_{HCl} molar ratio of 40, and the results are shown in Figure 1S (Supporting Information). It is also interesting to note that the specific surface area, specific pore volume, pore diameter and pore wall thickness of MnSBA-15(295H) are higher as compared to those of other MnSBA-15 and pure silica SBA-15 materials (Table 1) because the Mn species in MnSBA-15(295H) values are higher than those of other MnSBA-15. Particularly, MnSBA-15 has higher pore diameter than SBA-15 because Mn species with oxygen has a higher bond length than Si−O. All these observations suggest that a high n_{H2O}/n_{HCl} molar ratio favors Mn incorporation into SBA-15 without affecting the textural order.

The ESR spectrums of calcined MnSBA-15 samples prepared with different water to hydrochloric acid molar ratios (n_{H2O}/n_{HCl}) are shown in Figure 3, exhibiting a typical Mn^{2+} signal, sextet lines with a hyperfine coupling constant of 9.4 mT, and $g \approx 2.00$. Each sample prepared here gave an almost similar spectrum but which rose in intensity with increasing n_{H2O}/n_{HCl} molar ratio from 40 to 295. It should be noted that the all spectrums in Figure 2 are similar to that reported by Zhao and Goldfarb,[28] the Mn-ions are within the pores, and also there is resultant increase in the number of Lewis acid sites. Moreover, the intensity of MnSBA-15(295H) is higher than that of other MnSBA-15 due to a high loading of Mn-ion into SBA-15. On the basis of the results, for all samples, it is inferred that the Mn^{2+} is coordinated to Si(IV) by distorted octahedral environments.

Figure 4 shows several representative field emission-scanning electron microscopy (FE-SEM) images for mesoporous MnSBA-15(295H). The morphology of MnSBA-15(295H) can be controlled by the simple adjustment of the molar n_{H2O}/n_{HCl} ratio to 295 at a fixed n_{Si}/n_{Mn} ratio of 4 in the synthesis gel, resulting in the morphology as rope-like hexagonal mesoporous material. The MnSBA-15 can have a long rope-like aspect of as much as several hundred micrometers that is made up of a bundle of ropes of diameter ~10 μm, as shown in Figure 2S (see Supporting Information).

Transmission electron microscopy (TEM) images show well-ordered hexagonal arrays of 1D mesoporous channels and further confirm that MnSBA-15 samples have a 2D *p6mm* hexagonal structure. Figure 5 shows the TEM images of the MnSBA-15(295H) sample. The distance between two consecutive centers of hexagonal pores estimated from the TEM image is ca. 12 nm. The average thickness of the wall is ca. 3.7 nm, which is much larger than that for MCM-41, and its pore diameter is around 8.6 nm, in agreement with the N_2 adsorption measurements. The above results of ICP-AES, XRD, N_2

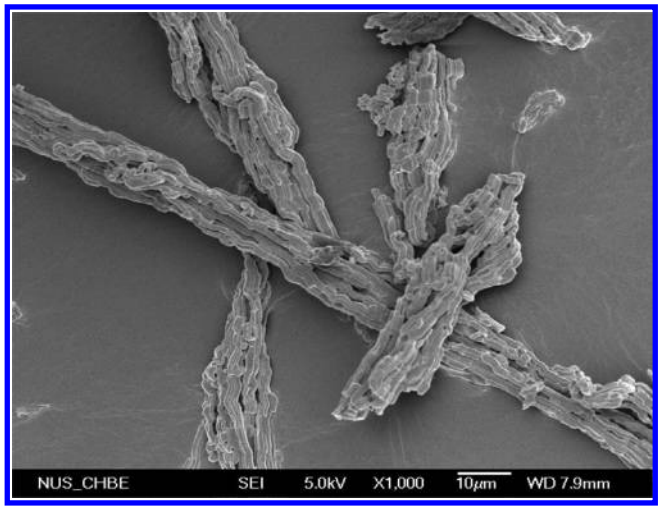

Figure 4. FE-SEM micrograph of calcined MnSBA-15(295H).

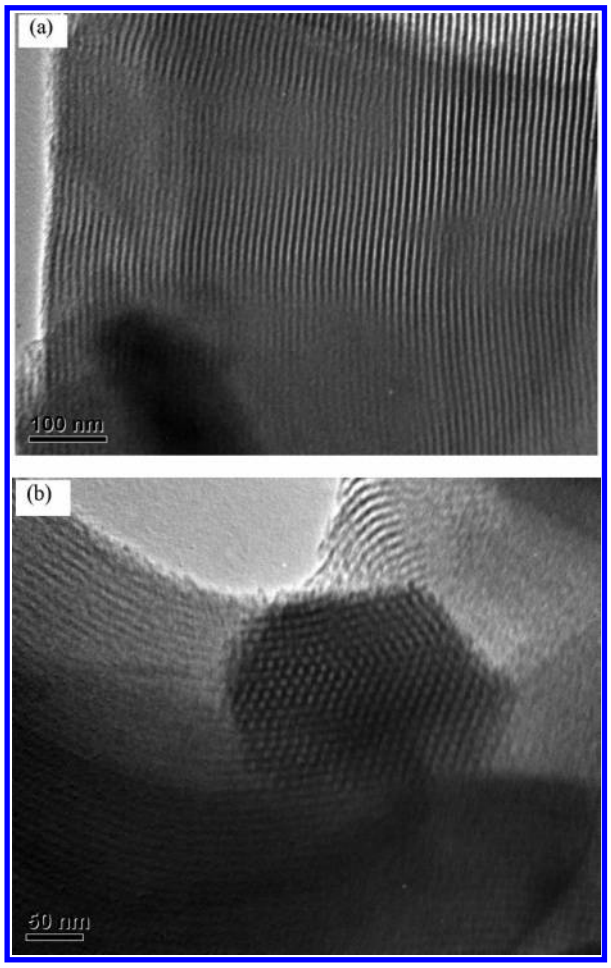

Figure 5. TEM micrographs of calcined MnSBA-15(295H).

adsorption, FE-SEM, and TEM suggest a successful isomorphous substitution of a higher amount of Mn species into the siliceous framework of SBA-15 under a direct pH adjusting method without affecting of structural and textural order.

Effect of n_{Si}/n_{Mn} Ratios. The elemental compositions of calcined MnSBA-15 materials synthesized with different n_{Si}/n_{Mn} ratios at a fixed n_{H2O}/n_{HCl} molar ratio are listed in Table 1. In all cases, the n_{Si}/n_{Mn} ratios of the calcined MnSBA-15 materials in the product are lower than the n_{Si}/n_{Mn} ratio in the synthesis gel. This could be due to the high solubility of the Mn precursors in the acidic hydrothermal synthesis conditions.

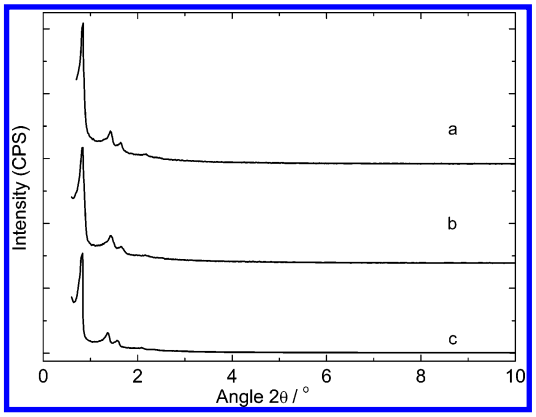

Figure 6. XRD powder patterns of calcined MnSBA-15 materials prepared with different n_{Si}/n_{Mn} ratios: (a) MnSBA-15(26), (b) MnSBA-15(10), and (c) MnSBA-15(4).

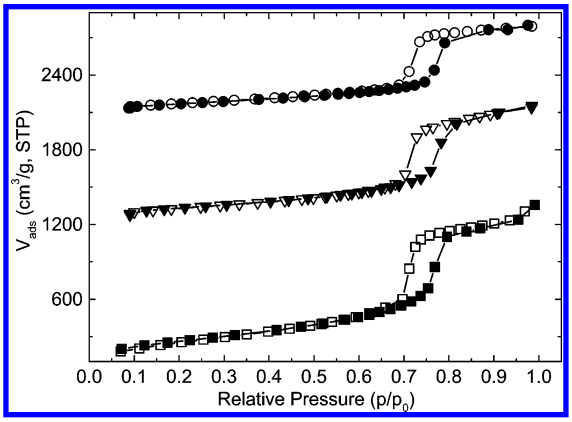

Figure 7. Nitrogen adsorption isotherms of calcined MnSBA-15 materials prepared with different n_{Si}/n_{Mn} ratios (closed symbols, adsorption; open symbols, desorption): (■) MnSBA-15(4), (▼) MnSBA-15(10), and (●) MnSBA-15(26). (For the value of shift of each isotherm, the values of relative pressure (p/p_o) are 6.72, 6.61, and 6.53 for MnSBA-15(4), MnSBA-15(10), and MnSBA-15 (26), respectively.)

Although the n_{Si}/n_{Mn} molar ratios from 99.6 to 7.3 increases in this synthesis method.

Figure 6 shows the powder XRD patterns of calcined MnSBA-15 samples synthesized with different n_{Si}/n_{Mn} ratios. All samples show that five well-resolved peaks are indexed to the (100), (110), (200), (210), and (300) reflections. Interestingly, the intensity of the XRD peaks shifts to lower angle in 2θ, and the unit cell parameter for the samples increase with decreasing n_{Si}/n_{Mn} ratio due to increasing Mn incorporation (Table 1). This indicates that the structural order can be improved with Mn species incorporation into the SBA-15 framework.

Figure 7 shows the nitrogen adsorption isotherms of calcined MnSBA-15 samples synthesized with different n_{Si}/n_{Sn} ratios. All isotherms show a sharp condensation step at relative pressures in the range of 0.63−0.91. It can also be seen that the capillary condensation step is shifted to higher relative pressures with increasing Mn species content in the product. This corresponds to an increase of the pore diameter as the Mn species content of the samples increase while their pore volume and pore wall thickness increase at the expense of the specific surface area as expected for cylindrical pores (Table 1). Unit cell size and pore diameter decrease with increasing n_{Si}/n_{Mn} ratio of the product (Table 1). The same effect has been found when manganese acetate tetrahydrate is used as the Mn source in the synthesis of MnMCM-41.[28] It is obvious that the enlargement of the unit cell size is not a consequence of Mn introduction into the walls since the unit cell size enlargement is limited to

the use of manganese nitrate tetrahydrate as the Mn source. Because both Mn sources have the divalent Mn species, the observed pore size enlargement in MnSBA-15 prepared from manganese nitrate tetrahydrate could be explained. Generally, in the crystalline zeolites, metal-ion incorporation slightly increases the pore size because of its longer bonding length with oxygen than Si−O. However, there is no regular rule in SBA-15 as it has an amorphous structure where both bond length and angle may change. Usually, it has been observed that the pore size of SBA-15 decreases after metal-ion incorporation, but there is no clear explanation for this observation. SBA-15 has thicker pore walls relative to zeolites so that the incorporated metal-ion cannot be substituted into the silica framework completely. That is, a part of the metal-ion will be exposed on the pore wall surface so that it might have properties similar to impregnated metal-ion complexes on the SBA-15 walls. The incorporated metal-ion may interact with surface hydroxyl groups and may contract the pore wall when combined with two or three hydroxyl groups, so that the pore size decreases.[29,30] If these metal-ions are deeply incorporated within the silica framework, this pore shrinkage might not occur as with condensed surface hydroxyl groups, and the pore size might be increased instead by the increased metal−oxygen bond length, as for zeolites. In this study, the pore size increases after Mn-ion incorporation as shown in Table 1. This is an unusual result, and strongly suggests that Mn-ions are incorporated into silica framework according to the above hypothesis. Moreover, it is shown that the pore size enlargement occurs without any ascertainable change in the structural order of the materials with increasing the Mn-ions in the synthesis gel. In addition, all materials prepared with various n_{Si}/n_{Mn} ratios from 26.3 to 2.2 (Table 1) possess higher pore volumes as compared to those of the pure silica SBA-15 materials, thus indicating a high fraction of (ultra)micropores in the MnSBA-15 samples. This indicates that MnSBA-15 materials can be prepared with very high Mn species content ($n_{Si}/n_{Mn} = 2.2$, see Table 1) without affecting the textural order of the materials.

Figure 3c−e shows the ESR spectra of calcined MnSBA-15 samples prepared with different n_{Si}/n_{Mn} ratios. The intensity of ESR spectra increases with decreasing molar ratio of n_{Si}/n_{Mn} because a higher number of Q_3 silanol groups are strongly bonded with Mn species. The intensity of MnSBA-15(4) is higher than that of other MnSBA-15 due to a greater Mn species incorporation. The Mn^{2+} species in different n_{Si}/n_{Mn} ratios of MnSBA-15 samples are coordinated on the silica pore walls by distorted octahedral environments. A similar behavior has also been reported for MnMCM-41 materials.[28]

Effect of Synthesis Temperature. Zhao et al.[13] reported that the unit cell size and pore diameter of SBA-15 materials can be increased by variation of the synthesis temperature from 383 to 403 K. Here, we report that the synthesis of MnSBA-15 is conducted with the same synthesis temperature. The XRD powder patterns for these materials are very well-defined and characteristic of well-ordered hexagonal materials (Figure 8A). While the XRD reflection peaks are seriously shifted to lower 2θ values when the synthesis temperature is systematically increased from 373 to 403 K, and the unit cell size expands (Table 1). Moreover, at higher synthesis temperature (403 K), the intensity of reflection peaks in the MnSBA-15(403 K) indicates that the material possesses thinner walls as suggested by Zhao et al.[13] for the analogous hexagonal structure of pure silica SBA-15. It is interesting to note that the structural orders of the MnSBA-15 materials are maintained up to the synthesis temperature of 403 K. The results of n_{Si}/n_{Mn} ratios of all

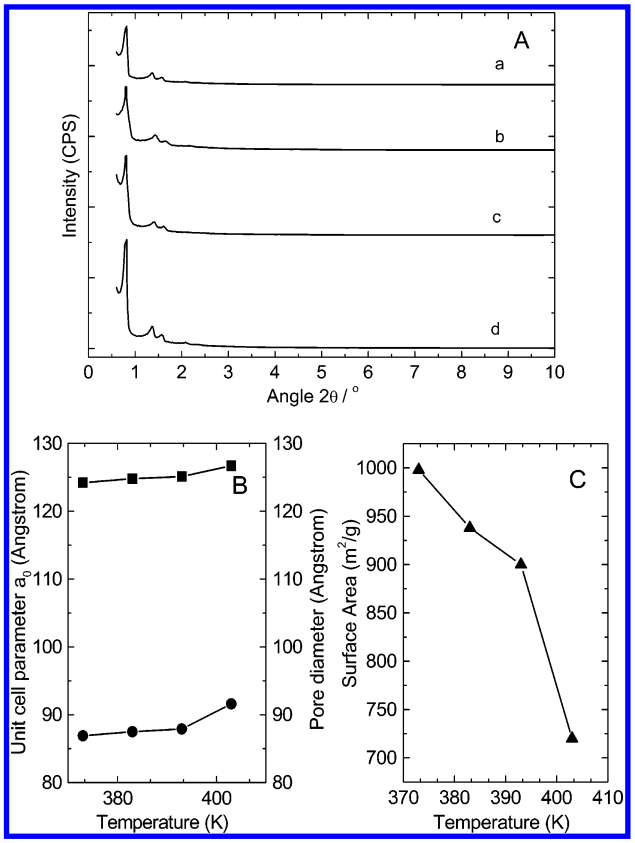

Figure 8. (A) XRD powder patterns of calcined MnSBA-15 materials prepared at different temperatures: (a) MnSBA-15(403 K), (b) MnSBA-15(393 K), (c) MnSBA-15(383 K), and (d) MnSBA-15(373 K). (B and C). Evaluation of unit cell parameter, pore diameter, and surface area with different synthesis temperatures in gel at a fixed n_{Si}/n_{Mn} ratio of 4: (■) unit cell parameter, (●) pore diameter, and (▲) surface area.

MnSBA-15 samples in different temperature synthesis can be found by ICP-AES. On the basis of the results, it should be pointed out that the incorporation of Mn species on the silica walls could not be affected by increasing the synthesis temperature (Table 1).

For the corresponding samples the textural properties are shown in Table 1. For these samples, the position of the capillary condensation step shifts to higher relative pressure when the synthesis temperature is increased from 373 K to 403 K. Moreover, the amount of N_2 adsorbed also increases with synthesis temperature (not shown in the figure). The textural properties obtained from examination of the nitrogen isotherms of MnSBA-15 prepared at different temperatures are summarized in Table 1. With increasing temperature, specific pore volume (1.12−1.16 cm^3/g) and pore diameter (86.9−90.6 Å) increase whereas the specific surface area (998−720 m^2/g) and pore wall thickness (37.3−34.1Å) decrease. Figure 8B,C show the pore size, unit cell parameter, and surface areas of MnSBA-15 with different synthesis temperatures. Then, an increase the pore diameter and unit cell parameter, and a decrease the surface areas with increasing crystallization temperature are confirmed by the results of N_2-adsorption and XRD.

An increase the unit cell size and pore diameter, and a decrease the specific surface area and wall thickness of MnSBA-15 materials with increasing synthesis temperature can be clearly observed and might be explained as follows: the nature of the copolymer blocks can be changed with different synthesis temperature.

In nature, the copolymer poly(ethylene oxide) (PEO) blocks are hydrophilic, and the poly(propylene oxide) (PPO) blocks

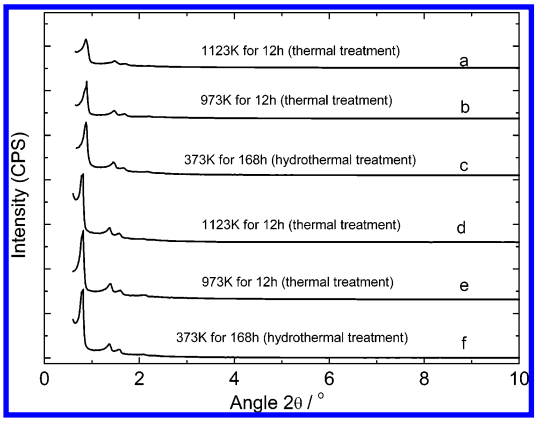

Figure 9. XRD powder patterns of MnSBA-15 materials prepared after hydrothermal and thermal treatment: (a−c) MnSBA-15(26) and (d−f) MnSBA-15(295H). (Hydrothermal: One gram of sample was treated in pure boiling water at 373 K for 168 h. Thermal: Two grams of sample was treated at different temperatures with various times.)

are hydrophobic. In acidic hydrothermal synthesis conditions, the size of copolymer systematically increases with gradually increasing synthesis temperature from 373 to 403 K, while, for the formation of large pore of MnSBA-15, it interacts with the silanol groups via hydrogen bonds, then the silanol groups interact with Mn species by adjusting the water to hydrochloric acid ratios. The copolymer size increases by the following reasons: in higher reaction temperatures, the length of hydrophobic part of copolymer increases by interacting a greater number of hydrophilic PEO blocks with hydrophobic PPO blocks. Hence, the hydrophilicity of PEO blocks decreases while they become more hydrophobic than PPO in a higher synthesis temperature (403 K). In the present conditions, the PEO blocks are expected to interact more closely associated with inorganic walls than the more hydrophobic PPO blocks. Hence it is believed that PEO blocks are responsible for the formation of micropores in the SBA-15 framework.[13] The above variation of the copolymer size with increasing the temperature from 373 to 403 K is also reflected in a substantial broadening of the pore size distribution of the MnSBA-15 materials (not shown in the figure).

Hydrothermal and Thermal Stabilities. To evaluate the hydrothermal and thermal stabilities, MnSBA-15(295H) and MnSBA-15(26) materials were treated in boiling water at 373 K for 168 h in autogenous pressure while the corresponding samples were thermal treated at 973 K for 12 h and 1123 K for 24 h in oxygen atmosphere. The distinct structural parameters might be helpful for better understanding the factors that affect the hydrothermal and thermal stabilities of MnSBA-15 materials because the materials can be used as catalysts to synthesize a bulk aromatic molecule in chemical industries. The powder XRD pattern samples are shown in Figure 9. These materials possess highly ordered two-dimensional hexagonal mesostructures with uniform cylindrical channels. The structural parameters of these samples are listed in Tables 1S and 2S (see Supporting Information). It can be seen that each sample has distinct structural parameters.

Figure 9 shows XRD patterns of MnSBA-15 samples after being treated in boiling water at 373 K for 168 h and thermal treated at 973 K for 12 h and 1123 K for 12 h. After hydrothermal and thermal treatment, the (100) diffraction peak of MnSBA-15(126) sample shifts to a higher 2θ degree, and the relative intensity of diffraction peaks decreases, resulting in the disappearance of the (210) and (300) diffraction peaks while the unit cell parameter decreases because it has a high number of free Si−O−Si bonds due to a low amount of Mn-ion incorporation, and the results are given in Tables 1S and 2S (see Supporting Information). The results suggest that the hydrothermal treatment for MnSBA-15(26) may cause somewhat shrinkage of mesopores and structural disorder. Nevertheless, MnSBA-15(26) still displays three strong and well-resolved peaks, indexed as (100), (110), and (200) diffraction peaks of *P6mm* symmetry, suggesting a highly ordered mesostructure.[31] But, after hydrothermal and thermal treatment, the unit cell parameters of MnSBA-15(295H) remain constant, because the Si−O−Mn bonds are relatively stable to further attack by boiling water and thermal temperature due to thicker pore walls by the greater Mn-ion incorporation. The results are given in Tables 1S and 2S.

The remarkable improvement of hydrothermal and thermal stabilities due to the higher Mn-ion incorporation is further evidenced by the measurement of N_2 adsorption, and the results are shown in Tables 1S and 2S. The textural properties of the MnSBA-15 materials are measured after they have been treated in boiling water for 168 h and thermal treated in different temperatures with various times. The surface area of the MnSBA-15(26) sample decreases from 1079 to 900 m^2/g while its pore diameter, pore volume, and pore walls thickness decreases when two or more surface hydroxyl groups combined, but the surface area, pore diameter, pore volume, and pore walls thickness in MnSBA-15(295H) sample could not so much decrease. Here, the Si−O−Mn bonds are also relatively stable to further attack from boiling water and thermal temperature due to the higher number of Mn-ions in the framework on the silica pore walls;[32] the presence of Mn^{2+} creates a negative charge on the surface of the pore walls, repelling OH^- ions and therefore preventing the hydrolysis of siloxane bonds and also resulting in an increase in the number of acid sites. The textural properties in the MnSBA-15(26) sample decreases due to low amount of Mn-ion incorporation as it does not create a sufficient amount of negative charges on the surface of the pore walls. But the surface area of MnSBA-15(295H) sample remains constant due to creating the higher number of negative ions on the pore walls. Hence, it is concluded that Mn is irreversibly incorporated into the structure of the MnSBA-15(295H) sample. So the hydrothermal and thermal stabilities in MnSBA-15(295H) are higher than those in MnSBA-15(26). Finally, the results further confirm that the silica walls become thicker by a more Mn^{2+} framework on silica walls, and MnSBA-15(295H) sample also shows good hydrothermal and thermal stabilities.

The ESR studies describe that the Mn species incorporation and their coordination on silica surface could not be changed after thermal and hydrothermal treatment, and they are shown in Figure 3a,b. Figure 2S shows the hexagonal rope-like morphology of MnSBA-15(295H) after thermal treatment at 1123 K for 12 h. Finally, we found that the MnSBA-15(295H) has good hydrothermal and thermal stabilities with well-ordered hexagonal morphology.

Epoxidation of *trans*-Stilbene. The epoxidation of *trans*-stilbene (TS) with *tert*-butylhydrogenperoxide (TBHP) is the radical oxidation mechanism.[25] The active oxygen species on metal reacts with stilbene to yield an intermediate radical which has a long enough lifetime to rotate around the single carbon bond and isomerize. Thus, the thermodynamically stable trans isomer could become the major product, *trans*-stilbene oxide (TSO) and a part of the intermediates would undergo the reverse reaction to give *trans*-stilbene. Here the MnSBA-15 materials were tested as catalysts in the above reaction.

TABLE 2: Epoxidation of *trans*-Stilbene for Different Catalysts[a]

catalysts	yield (%) TSO	B	BA	conv. (%)	TSO selectivity (%)	n_{Si}/n_{Mn}[b]
MnSBA-15(295H)	97.6	0.6	0.2	98.4	99.18	2.2
MnSBA-15(4)	78.4	1.8	0.4	80.6	97.27	4.4
MnSBA-15(10)	68.3	3.9	1.0	70.3	97.15	10.6
MnSBA-15(26)	58.4	5.0	2.2	65.6	89.00	26.5
MnSBA-15(295H)[c]	97.6	0.6	0.2	98.4	99.18	2.2
MnSBA-15(295H)[c]	97.5	0.4	0.2	98.5	98.98	2.3
MnSBA-15(295H)[c]	97.6	0.6	0.2	98.5	99.08	2.2
MnSBA-15(295H)[c]	97.7	0.7	0.2	98.6	99.08	2.2
MnSBA-15(26)[c]	58.4	5.0	2.2	65.6	89.00	26.5
MnSBA-15(26)[c]	58.3	5.0	2.2	65.5	89.00	26.5
MnSBA-15(26)[c]	58.4	5.0	2.2	65.6	89.00	26.6
MnSBA-15(26)[c]	58.5	5.0	2.1	65.6	89.17	26.5
absence of catalyst	0	0	0	0	0	−

[a] Reaction conditions: 0.2 g of catalyst; $T = 338$ K; $t = 24$ h; *trans*-stilbene and TBHP mmol ratio = 1:10; solvent ratio = MeCN (9 mL):DMF (1 mL). [b] Results were obtained by ICP-AES after the reaction. [c] The used MnSBA-15 catalysts were reactivated in oxygen atmosphere at 773 K for 6 h for recycling experiments; TS, *trans*-stilbene; TSO, *trans*-stilbene oxide; B, benzaldehyde; BA, benzoic acid.

TABLE 3: Epoxidation of *trans*-Stilbene with Different Optimal Conditions over 0.2 g of MnSBA-15(295H)[a]

S no.	T (K)	t (h)	TS (mmol)	oxidant (mmol)	solvent (ml)	yield (%) TSO	B	BA	conv (%)	TSO selectivity (%)
1	328	24	1	THBP (10)	MeCN:DMF (9:1)	47.4	0.6	0.2	48.2	98.34
2	338	24	1	THBP (10)	MeCN:DMF (9:1)	97.6	0.6	0.2	98.4	99.18
3	363	24	1	THBP (10)	MeCN:DMF (9:1)	55.4	8.5	3.6	67.5	82.07
4	338	72	1	THBP (10)	MeCN:DMF (9:1)	97.8	0.6	0.2	98.6	99.18
5	338	96	1	THBP (10)	MeCN:DMF (9:1)	98.5	0.3	0.1	98.9	99.59
6	338	24	1	THBP (5)	MeCN:DMF (9:1)	49.3	10. 0	5.0	64.3	76.67
7	338	24	2	THBP (5)	MeCN:DMF (9:1)	38.4	6.8	6.3	51.5	74.56
8	338	24	3	THBP (10)	MeCN:DMF (9:1)	32.3	4.7	4.7	41.7	77.45
9	338	24	1	THBP (10)	MeCN:DMF (9:9)	53.5	5.4	2.5	61.4	87.13
10	298	24	1	THBP (10)	MeCN:DMF (9:1)	11.2	1.2	1.0	13.4	83.58
11	298	24	1	H_2O_2 (10)	MeCN:DMF (9:1)	0	0	0	0	0
12	298	24	1	PhIO (10)	MeCN:DMF (9:1)	9	2.0	0.3	11.3	79.64
13	338	24	1	O_2 (excess)	MeCN:DMF (9:1)	0	0	0	0	0
14	338	24	1	THBP (10)	MeCN (10)	19.1	1.4	1.0	21.5	88.83
15	338	24	1	THBP (10)	DMF (10)	14.7	1.5	0.4	16.6	88.55
16	338	24	1	THBP (10)	THF (10)	7.6	1.0	0.5	9.1	83.51
17	338	24	1	THBP (10)	MeOH (10)	8.5	1.3	0.4	10.2	83.33

[a] T, temperature; t, time; TS, *trans*-stilbene; TSO, *trans*-stilbene oxide; B, benzaldehyde; BA, benzoic acid.

The epoxidation of TS was carried out with 1:10 mmol ratio of $n_{trans-stilbene}/n_{TBHP}$ and 9:1 solvent ratio (v/v) of n_{MeCN}/n_{DMF} at 338 K for 24 h over MnSBA-15 catalysts for selective synthesis of TSO, and the results are shown in Table 2. Only traces amount of benzaldehyde (B) and benzoic acid (BA) were observed. It has been found that the activity of the catalysts changes in the following order: MnSBA-15(295H) > MnSBA-15(4) > MnSBA-15(10) > MnSBA-15(26). MnSBA-15(295H) exhibits the best performance with a TS conversion of 98.4% and a TSO yield and selectivity of 97.6 and 99.1%, respectively, which are significantly higher as compared to other mono and/or bimetal substituted uni-dimensional mesoporous materials such as MnMCM-41 and ZrMnMCM-41under optimized reaction conditions [2,25] (see Table 3S in Supporting Information). It should be noted that the uni-dimensional MnMCM-41(31) catalyst gives a TS conversion of only 70.4% and a TSO yield of 57.5% under comparable reaction conditions.[25] The observed higher activity of MnSBA-1(295H) is tentatively ascribed to its two-dimensional space and high loading of Mn^{2+}-ion on the inner pore structure framework resulting in a higher number of accessible active sites, because the Mn^{2+}-ions produce a high number of Lewis acid sites on the inner surface of pore walls. Especially, the superior catalytic activity of MnSBA-15 catalyst toward TS epoxidation is attributed to their active oxygen with a high electron affinity (electrophilic) for attacking of the electron-rich double bond of the stilbene molecule. Based on the catalytic results, it is interesting to note that most Mn^{2+}-ion might be dispersed on the inner surface of the silica pore walls. As MnSBA-15(295H) is the most active catalyst in this work, for furthermore study we have chosen this catalyst due to the confirmation of the best optimal conditions (temperature, time, etc.).

For the best optimal conditions for highly selective synthesis of TSO over MnSBA-15(295H), the reaction was carried out using the different optimal conditions such as reaction temperature, reaction time, and mmol ratios of reactant (*trans*-stilbene:TBHP). Solvent molar ratios were also investigated using different oxidants and solvents.

The epoxidation of TS was carried out with various temperatures using 1:10 mmol ratio of $n_{trans-stilbene}/n_{TBHP}$ and 9:1 solvent ratio (v/v) of n_{MeCN}/n_{DMF} for 24 h over MnSBA-15(295H), and the results are shown in Table 3 (S. No. 1−3). The optimum temperature is found to be 338 K. Deviation to either side of the required temperature shows that the TS conversion, TSO yield, and selectivity decreases. Lower temperatures (<328 K) do not favor the formation of TSO because the catalytic activity of all catalysts are less. At higher temperature (>363 K), the TS conversion, TSO yield, and selectivity decreases. This may be due to the formation of byproduct such as benzaldehyde (B) and benzoic acid (BA) involving carbon−carbon double bond cleavage between the two aromatic rings in the TS. The TSO yield and selectivity is found to be 97.6% and 99.18%,

respectively, at 338 K for 24 h in the presence of MnSBA-15-(295H). Thus, MnSBA-15(295H) has a higher yield and selectivity of *trans*-stilbene oxide than other MnSBA-15, Mn-MCM-41, and ZrMnMCM-41.[2,25]

The epoxidation of TS was carried out with different reaction times using 1:10 mmol ratio of $n_{\text{trans-stilbene}}/n_{\text{TBHP}}$ and 9:1 solvent ratio (v/v) of $n_{\text{MeCN}}/n_{\text{DMF}}$ at 24 h over MnSBA-15(295H), and the results are shown in Table 3 (S. No. 2, 4, 5). The TS conversion, TSO yield, and selectivity slightly increases with increasing reaction time, because the catalytic activity on the surface of the inner pore walls may be slightly increased depending upon the pore structure. The TS conversion, TSO yield, and selectivity was found to be 98.4%, 97.6%, and 99.1%, respectively, for 24 h at 338 K over MnSBA-15(295H). On the basis of the results, it is interesting to note that the suitable reaction time is 24 h for highly selective synthesis of TSO.

Liquid-phase epoxidation of TS was carried out with various ratios of $n_{\text{trans-stilbene}}/n_{\text{TBHP}}$. In all the cases, TSO is obtained as the major product along with small amounts of B and BA as byproducts. It is observed that, at a reaction temperature of 338 K at 24 h, the highest TS conversion (98.4%) and TSO yield (97.6%) and selectivity (99.18%) are obtained at a $n_{\text{trans-stilbene}}/n_{\text{TBHP}}$ ratio of 1/10 over MnSBA-15(295H) as can be seen in Table 3 (S. No. 2, 6−8). As the mmol ratio of TBHP is increased up to 10 with standard TS of 1 mmol, the TS conversion and TSO yield and selectivity increase, but the conversion, yield, and selectivity decrease after 10 mmol (>10 mmol), and as the mmol ratio of TS is increased (>3 mmol), the conversion, yield, and selectivity decrease. This may be due to coke formation of the catalyst; that is why reactant ratios are unsaturated on the catalyst surface. Hence, the optimal mmol ratio of $n_{\text{trans-stilbene}}/n_{\text{TBHP}}$ is 1:10. Thus, the optimum conditions for obtaining maximum TS conversion and the highest TSO selectivity can be summarized as follows: catalyst, MnSBA-15(295H); reaction temperature, 338 K; reaction time, 24 h; *trans*-stilbene to TBHP mmol ratio, 1:10.

Various oxidants viz. hydrogen peroxide (H_2O_2), TBHP, iodosobenzene (PHIO), and gaseous oxygen (O_2) were examined as oxidant for catalytic epoxidation of TS over MnSBA-15-(295H), and the results are summarized in Table 3 (S. No. 2, 11−13). Upon the introduction of H_2O_2 at ambient temperature, a bubbling occurs in the MnSBA-15(295H) and no reaction of TS is observed. It is clear that H_2O_2 cannot be used as an oxidant at this temperature because of the rapid decomposition to O_2 with high exothermicity. PhIO could oxidize TS to the corresponding oxide, although the yield is not so high. In the case of TBHP, a little formation of TSO is detected at ambient temperature despite excess amount of oxidant used. The yield of TSO is improved to 97.6% by changing the reaction temperature to 338 K and is shown in Table 3 (S. No. 1−3, 10). The epoxidation reaction with gaseous O_2 at 338 K shows no reaction. TBHP is employed as an oxidant in the present study to increase in the yield of TSO.

The change in the catalytic epoxidation on MnSBA-15(295H) in the presence of different solvents was investigated, and the results are presented in Table 3 (S. No. 14−17). Since TBHP is added to the solution as a 70% aqueous solution, polar solvents such as tetrahydrofuran (THF), methanol (MeOH), acetonitrile (MeCN), and dimethylformamide (DMF) are used to avoid separation of the solvent during the reaction. The yield of TSO is in the order MeCN > DMF > MeOH >THP, indicating that MeCN is the best solvent for the epoxidation under the present conditions with significant TSO yield (19.1%). On the other hand, DMF is the next best solvent from the viewpoint of TSO yield (14.7%). It is a dipolar aprotic solvent, with high dielectric constant and electron donor properties and its ability to form of complexes. The findings suggest the possibility that the combination of two solvents might result in good activity, yield, and selectivity. Then the reaction was examined in various solvent molar ratio (MeCN:DMF), and the results are shown in Table 3 (S. No. 2, 9).

The highest yield (97.6%) and selectivity (99.10%) of TSO is achieved for a ratio of 9:1 (v/v) of MeCN and DMF. The provisional explanation is as follows. The low reaction rate and the excellent selectivity may be due to the strong interaction of a DMF molecule with active site. That is, the strong interaction would inhibit the coordination of the substrate and enhance desorption of the product from the active site. The affinity of DMF to the metal ion might promote separation of TSO from the site, which results in the prevention of deep oxidation of the oxide produced and in the increase in the selectivity.

MnSBA-15(295H) and MnSBA-15 (26) catalysts were reused for the epoxidation of TS using reactant as 1:10 mmol ratio of TS and TBHP with 9:1 solvent ratio (v/v) of MeCN and DMF at 338 K for 24 h, and the results have been depicted in Table 2. No loss of catalytic activity, and Mn species on the inner side surface of pore walls in MnSBA-15(295H) and MnSBA-15(26) is observed after 4 runs. Instead, its TS conversion, TSO yield, and selectivity remain constant with each cycling. Especially, for epoxidation of TS, the MnSBA-15(295H) is more suitable as an active catalyst than MnSBA-15(26) due to greater Mn incorporation on the silica walls. Thus, the MnSBA-15-(295H) catalyst is a better and very suitable catalyst for epoxidation of *trans*-stilbene than MnSBA-15(26), MnMCM-41, and ZrMnMCM-41.[2,25]

Conclusions

We developed a novel method to incorporate Mn species into the SBA-15 silica matrix with very high structural order and high Mn species content by simply adjusting the molar water to hydrochloric acid ratio in the gel mixture. It has been found that the $n_{\text{Si}}/n_{\text{Mn}}$ ratio of the MnSBA-15 materials can be prepared up to $n_{\text{Si}}/n_{\text{Mn}}$ ratio of 2.2 by varying the molar water to hydrochloric acid ratio and $n_{\text{Si}}/n_{\text{Mn}}$ ratio in the synthesis gel. ICP-AES results show that the Mn species incorporation into SBA-15 in $n_{\text{H2O}}/n_{\text{HCl}}$ molar ratio of 295 is higher as compared to other $n_{\text{H2O}}/n_{\text{HCl}}$ molar ratios, and the $n_{\text{Si}}/n_{\text{Mn}}$ ratios in MnSBA-15 could not be affected when the crystallization temperature is increased from 373 to 403 K. XRD and N_2 adsorption studies show that the structural and textural properties of MnSBA-15 could be improved due to Mn incorporation on the silica walls while the pore size of MnSBA-15 can be increased from 86.9 to 90.6 Å with increasing crystallization temperature from 373 to 403 K without addition of any organic swelling agents. ESR studies confirm that the majority of the Mn-ions in MnSBA-15 exist in a distorted octahedral coordination environment (most probably occupying framework positions such as inner surface of pore walls). FE-SEM and TEM studies confirm that the MnSBA-15 samples have a long rope-like morphology and uniform pore diameter. The catalytic activity of the novel catalyst is investigated in the epoxidation of *trans*-stilbene reaction. MnSBA-15 is found to be more active and recyclable than previously studied systems such as ZrMnMCM-41 or MnMCM-41. The observed TS conversion of 98.4% (TSO yield, 97.6%; selectivity, 99.18%) in MnSBA-15(295H) is significantly higher as compared to other mono- and bimetal substituted uni-dimensional MCM-41 molecular sieves under optimized reaction conditions.[2,25]

Acknowledgment. The Singapore Millennium Fellowship (SMF) awarded by Singapore Millennium Foundation for M. Selvaraj (2005-SMF-0437) is gratefully acknowledged for this work.

Supporting Information Available: BJH pore size distributions for calcined MnSBA-15 materials prepared with different n_{H2O}/n_{HCl} ratios; FE-SEM images for MnSBA-15(295H); physicochemical characterization of MnSBA-15 after hydrothermal and thermal treatment; comparison of TS conversion and TSO yield and selectivity over MnSBA-15(295H) with other mesoporous catalysts. This material is available free of charge via the Internet at http://pubs.acs.org.

References and Notes

(1) Jorgensen, K. A. *Chem. Rev.* **1989**, *89*, 431
(2) Yonemitsu, M.; Tanaka, Y.; Iwamoto. M. *J. Catal.* **1998**, *178*, 207.
(3) García-Martínez, J.; Cazorla-Amorós, D.; Linares-Solano, A. *Appl. Catal., B* **2004**, *47*, 203.
(4) Sun, Q.; Sachtler, W. M. H. *Appl. Catal., B* **2003**, *42*, 393.
(5) Kresge, C. T.; Leonowicz, M. E.; Roth, W. J.; Vartuli, J. C.; Beck, J. S. *Nature* **1992**, *359*, 710.
(6) Sayari, A. *Chem. Mater.* **1996**, *8*, 1840.
(7) Corma, A. *Chem. Rev.* **1997**, *97*, 2373.
(8) Selvaraj, M.; Pandurangan, A.; Seshadri, K. S.; Sinha, P. K.; Krishnasamy, V.; Lal, K. B. *J. Mol. Catal. A* **2002**, *186*, 173.
(9) Selvaraj, M.; Pandurangan, A.; Seshadri, K. S.; Sinha, P. K.; Lal, K. B. *Appl. Catal., A* **2003**, *242*, 347.
(10) Selvaraj, M.; Sinha, P. K.; Seshadri, K. S.; Pandurangan, A. *Appl. Catal., A* **2004**, *265*, 75.
(11) Selvaraj, M.; Lee, T. G. *Microporous Mesoporous Mater.* **2005**, *85*, 39.
(12) Zhao, D.; Huo, Q.; Feng, J.; Chmelka, B. F.; Stucky, G. D. *J. Am. Chem. Soc.* **1998**, *120*, 6024.
(13) Zhao, D.; Feng, J.; Huo, Q.; Melosh, N.; Fredrikson, G.; Chmelka, B.; Stucky, G. D. *Science* **1998**, 279.
(14) Ryoo, R.; Kim, J. M.; Shin, C. H. *J. Phys. Chem.* **1996**, *100*, 17718.
(15) Yang, P.; Zhao, D.; Margolese, D.; Chmelka, B. F.; Stucky, G. D. *Chem. Mater.* **1999**, *11*, 2831.
(16) Yang, P.; Zhao, D.; Margolese, D.; Chmelka, B. F.; Stucky, G. D. *Nature (London)* **1998**, *396*, 152.
(17) Ying, Y. J.; Mehnert, C. P.; Wong, M. S. *Angew. Chem., Int. Ed. Engl.* **1999**, *38*, 56.
(18) (a) Yue, Y.; Gideon, A.; Bonardet, J.-L.; Melosh, N.; D′Espinose, J.-B.; Fraissard, J. *Chem. Commun.* **1999**, 1967. (b) Vinu, A.; Murugesan, V.; Bohlmann, W.; Hartmann, M. *J. Phys. Chem. B.* **2004**, *108*, 11496.
(19) (a) Nozaki, C.; Lugmair, C. G.; Bell, A. T.; Tilley, T. D. *J. Am. Chem. Soc.* **2002**, *124*, 13194. (b) Vinu, A.; Sawant, D. P.; Ariga, K.; Hossain, K. Z.; Halligudi, S. B.; Hartmann, M.; Nomura, M. *Chem. Mater.* **2005**, *17*, 5339.
(20) Luan, Z.; Bae, J. Y.; Kevan, L. *Chem. Mater.* **2000**, *12*, 3202.
(21) (a) Zhang, W.-H.; Lu, J.; Han, B.; Li, M.; Xiu, J.; Ying, P.; Li, C. *Chem. Mater.* **2002**, *14*, 3413. (b) Vinu, A.; Srinivasu, P.; Miyahara, M.; Ariga, K. *J. Phys. Chem. B.* **2006**, *110*, 801.
(22) Berrichi, Z. E.; Cherif, L.; Orsen, O.; Fraissard, J.; Tessonnier, J.-P.; Vanhaecke, E.; Louis, B.; Ledoux, M.-J.; −Huu, C. P. *Appl. Catal., A* **2006**, *298*, 194.
(23) Wu, S.; Han, Y.; Zou, Y.-C.; Song, J.-W.; Zhao, L.; Di, Y.; Liu, S.-Z.; Xiao, F.-S. *Chem. Mater.* **2004**, *16*, 486.
(24) Selvaraj, M.; Sinha, P. K.; Lee, K.; Ahn, I.; Pandurangan, A.; Lee, T. G. *Microporous Mesoporous Mater.* **2005**, *78*, 139.
(25) Selvaraj, M.; Seshadri, K. S.; Pandurangan, A.; Lee, T. G. *Microporous Mesoporous Mater.* **2005**, *79*, 261.
(26) Sayari, A.; Liu, P.; Kruk, M.; Jaroniec, M. *Langmuir* **1997**, *13*, 2499.
(27) Imperor-Clerc, M.; Davidson, P.; Davidson, A. *J. Am. Chem. Soc.* **2000**, *122*, 11925.
(28) Zhao, D.; Goldfarb, D. *Chem. Commun.* **1995**, 875.
(29) Pauly, T. R.; Liu, Y.; Pinnavaia, T. J.; Billinge, S. J. L.; Rieler, P. *J. Am. Chem. Soc.* **1992**, *114*, 8835.
(30) Morey, M.; Davidson, A.; Eckert, H.; Stucky, G. *Chem. Mater.* **1996**, *8*, 486.
(31) Zhang, F.; Yan, Y.; Yang, H.; Meng, Y.; Yu, C.; Tu, B.; Zhao, D. *J. Phys. Chem. B* **2005**, *109*, 8723.
(32) Han, Y.; Li, N.; Zhao, L.; Li, D.; Xu, X.; Wu, S.; Di, Y.; Li, C.; Zou, Y.; Yu, Y.; Xiao, F. S. *J. Phys. Chem. B.* **2003**, *107*, 7551.